

Comparisons of the radial distributions of core-collapse supernovae with those of young and old stellar populations^{*}

J. P. Anderson^{†1,2} and P. A. James²

¹*Departamento de Astronomía, Universidad de Chile, Camino El Observatorio 1515, Las Condes, Santiago, Casilla 36-D, Chile*

²*Astrophysics Research Institute, Liverpool John Moores University, Twelve Quays House, Egerton Wharf, Birkenhead, CH41 1LD, UK*

ABSTRACT

We present observational constraints on the nature of core-collapse supernovae through an investigation into their radial distributions with respect to those of young and old stellar populations within their host galaxies, as traced by H α emission and R -band light respectively. We discuss results and the implications they have on the nature of supernova progenitors, for a sample of 177 core-collapse supernovae.

We find that the radial positions of the overall core-collapse population closely follow the radial distribution of H α emission, implying that both are excellent tracers of star formation within galaxies. Within this overall distribution we find that there is a central deficit of SNI which is offset by a central excess of SNIb/c. This implies a strong metallicity dependence on the relative production of the two types, with SNIb/c arising from higher metallicity progenitors than SNI. Separating the SNIb/c into individual classes we find that a trend emerges in terms of progenitor metallicity going from SNI through SNIb to SNIc, with the latter arising from the highest metallicity progenitors.

Key words: stars: supernovae: general – galaxies: general – galaxies: statistics

1 INTRODUCTION

Determining the characteristics of supernova (SN) progenitors is a key area of research given their importance and influence on many other astrophysical processes. The distribution of SNe within host galaxies can give substantial information as to the nature of their progenitors. At different galactocentric radii within galaxies different stellar populations are found with different mean ages and metallicities. One can therefore investigate how the radial distributions of SNe correlate with those of different stellar populations and use this to further constrain the nature of progenitor stars. Here we present results on the radial distribution of a large number of core-collapse (CC) SNe with respect to the R -(or r')-band light and H α emission of their host galaxies, and discuss the implications these have on the nature of SN progenitors. Results from an initial data set were presented in James & Anderson (2006) (JA06 henceforth) which showed that SNIb/c tended to occur within more central parts of the light distribution of their host galaxies, albeit

with small number statistics (only 8 SNIb/c). This was ascribed to SNIb/c arising from higher metallicity progenitors. We test these initial results with an increased sample size enabling us to distinguish between the various SN sub-types, and present further results from a combined sample of 115 SNI, 58 SNIb/c and 4 SN ‘impostors’.

1.1 Core-collapse supernova progenitors

CC SNe are thought to arise from stars with initial masses $>8 M_{\odot}$ (a value that has been converged upon from progenitor direct detections: Smartt et al. 2009, and the maximum observed masses of WDs: Williams et al. 2009). The different CC SN types are then thought to arise as a result of processes dependent on progenitor mass, metallicity and/or binarity. CC SNe are classified according to the presence/absence of spectral lines in their early time spectra, plus the shape of their light curves (see Filippenko 1997, for a review of SN classification). The first major classification comes from the presence of strong hydrogen emission in the SNI. SNIb and Ic lack any detectable hydrogen emission, while SNIc also lack the helium lines seen in SNIb. SNI can also be separated into various sub-types. SNIIP and IIL are classified in terms of the decline shape of their light curves (Barbon et al. 1979; plateau in the former and linear in the latter), thought to indicate different masses of their envelopes prior to SN, while SNIIn show narrow emission lines within their spectra (Schlegel 1990), thought to arise from interaction of the SN ejecta with a slow-moving circumstellar medium (e.g. Chugai & Danziger 1994). SNIib are thought to be

^{*} Based on observations made with the Isaac Newton Telescope operated on the island of La Palma by the Isaac Newton Group in the Spanish Observatorio del Roque de los Muchachos of the Instituto de Astrofísica de Canarias, and on observations made with the Liverpool Telescope operated on the island of La Palma by Liverpool John Moores University in the Spanish Observatorio del Roque de los Muchachos of the Instituto de Astrofísica de Canarias with financial support from the UK Science and Technology Facilities Council.

[†] E-mail: anderson@das.uchile.cl

intermediate objects between the SNII and Ib as at early times their spectra are similar to SNII (prominent hydrogen lines), while at later times they appear similar to SNIb (Filippenko et al. 1993). The main advances in our understanding of CC SN progenitors over the past decade have come from the direct detection of progenitor stars on pre-explosion images. A recent compilation of a decade long search for SN progenitors was presented by Smartt et al. (2009). One of the main conclusions from this work was a mass range for the production of SNIIP of between 8.5 and 16.5 M_{\odot} . However, the statistics on any of the other CC types currently preclude any firm conclusions as to the exact nature of their progenitors. Their spectral and light curve characteristics indicate that they must have lost some (the various II sub-types) or all (SNIb) of their hydrogen envelopes during their pre-SN evolution, with SNIc additionally having lost all helium. Whether this is due to different mass ranges of progenitors producing stronger stellar winds and thus removing increasing amounts of mass, or whether metallicity or binarity play a dominant role in deciding SN type is still under debate.

In the previous paper in this series (Anderson & James 2008, AJ08 henceforth) we concluded that the main CC SN types form a sequence of increasing progenitor mass, going from SNII to SNIb and SNIc, with the latter arising from the highest mass progenitors. Meanwhile there is also increasing evidence that SNIb/c tend to arise in more metal rich host galaxies than SNII (Prantzos & Boissier 2003, Prieto et al. 2008). It therefore seems likely that both progenitor mass and metallicity play important roles in producing the diversity of observed types. Stellar modeling also predicts these dependencies (e.g. Heger et al. 2003, Eldridge & Tout 2004) for single star progenitors. There is also a strong likelihood that massive close binaries produce some of the range of CC SN types. Evidence for binarity has been claimed for both SN 1987A and SN 1993J (Podsiadlowski et al. 1990 and Nomoto et al. 1993; Podsiadlowski et al. 1993; Maund et al. 2004 respectively), while comparisons of the number ratio of SNII to SNIb/c with predictions from single star models and observations of massive stars in the local group (Massey 2003, Crowther 2007), would seem to suggest that the production of a significant fraction of SNIb/c from binaries is required. Therefore while we have yet to tie down the progenitors of the different CC SN types (apart from possibly the SNIIP) there seem to be many available avenues within our current understanding of stellar evolution to produce the observed SN diversity.

1.2 The radial distribution of supernovae

At different radial positions within galaxies, stellar populations with different characteristics are thought to dominate. For example in spiral galaxies the central regions may be dominated by the old stellar bulge while at larger radii younger stellar populations associated with spiral arms are likely to become relatively more dominant. The metallicities of particular stellar populations are also observed to strongly correlate with galactic radial position, with higher chemical abundances found in the centres, decreasing with radial distance. This characteristic is found in nearly all galaxy types with the steepest abundance gradients found in normal spirals (see Henry & Worthey 1999, for a review on this subject). One can therefore study the radial distributions of different SN types to look for implied differences in their parent stellar populations and their progenitor stars.

Following Bartunov et al. (1992), van den Bergh (1997) found

a suggestion that SNIb/c are more centrally concentrated than SNII, a result that has been confirmed with better statistics by Tsvetkov et al. (2004) and most recently Hakobyan (2008). This suggests a metallicity dependence in producing SNIb/c, consistent with the scenario where higher metallicity progenitors have stronger line driven winds (see e.g. Puls et al. 1996; Kudritzki & Puls 2000; Mokiem et al. 2007) and thus lose more of their pre-SN envelopes producing a higher fraction of SNIb/c. These studies generally normalise the SN galactocentric distances to the total size of host galaxies in order to make statistical arguments on differences between the radial distributions of SN types. However, this analysis does not take into account how the *stellar populations* of these host galaxies are radially distributed and therefore complicates the interpretations that can be made on the nature of SN progenitors.

Here we use R -(or r')-band and $H\alpha$ imaging to investigate how the different SN types are radially distributed with respect to a young stellar population as traced by the $H\alpha$ emission and an older stellar population as traced by the R -(or r')-band continuum light. Using this analysis we address two questions. Firstly, are the radial positions of the different SN types consistent with being drawn at random from a young or an old stellar population? Secondly, do any of the SN types preferentially occur at particular radial positions within their host galaxies and what can this tell us about the nature of their progenitor ages and metallicities?

The paper is arranged as follows: in the next section we present the data and discuss the reduction techniques employed, in § 3 we summarise the radial aperture analysis used throughout this work, in § 4 we present the results for the radial distribution of the different SN types, in § 5 we discuss possible explanations for the results and implications that these have on the nature of SN progenitors and finally in § 6 we draw our conclusions.

2 DATA

The initial galaxy sample that formed the data set for JA06 was the $H\alpha$ Galaxy Survey ($H\alpha$ GS). This survey was a study of the SF properties of the local Universe using $H\alpha$ imaging of a representative sample of nearby galaxies, details of which can be found in James et al. (2004). 63 SNe were found to have occurred in the 327 $H\alpha$ GS galaxies through searching the International Astronomical Union (IAU) database ¹.

Through three observing runs on the Isaac Newton Telescope (INT) and a long term time allocation on the Liverpool Telescope (LT) we have now obtained imaging for the host galaxies of a total of 178 CC SNe, the analysis of which is presented here. The LT is a fully robotic 2m telescope operated remotely by Liverpool John Moores University. To obtain our imaging we used *RATcam* together with the narrow $H\alpha$ and the broad-band Sloan r' filters. Images were binned 2×2 to give $0.278''$ size pixels, and the width of the $H\alpha$ filter enabled us to image target galaxies out to ~ 2500 kms^{-1} . The INT observations used the Wide Field Camera (WFC) together with the Harris R -band filter, plus the rest frame narrow $H\alpha$ (filter 197) and the redshifted $H\alpha$ (227) filters enabling us to image host galaxies out to ~ 6000 kms^{-1} . During our 2005 INT observing run we also used the SII filter (212) as a redshifted $H\alpha$ filter and imaged 15 SN hosting galaxies at recession velocities of ~ 7500 kms^{-1} . The pixel scale on all INT images is $0.333''$ per

¹ <http://cfa-www.harvard.edu/iau/lists/Supernovae.html>

pixel and with both the LT and INT our exposure times were ~ 800 sec in $H\alpha$ and ~ 300 sec in R (or r' , for the remainder of this paper ‘ R -band’ will refer to both these filters, and the filter that was used for each target galaxy is listed in Table A1).

These additional SNe and host galaxies were chosen from the Padova-Asiago SN catalogue², as specific SN types were more complete for the listed SNe. At a later date all SN type classifications taken from the Padova-Asiago catalogue were checked through a thorough search of the literature and IAU circulars, as classifications can often change after the initial discovery and therefore those in the catalogue may not be completely accurate. The full list of SN types is given in Table A1, where references are given if classifications were changed from those in the above catalogue. The main discrepancies were the classification of the so-called SN ‘impostors’ as SNIIn in the Padova-Asiago catalogue. These are transient objects that are believed to be the outbursts from very massive Luminous Blue Variable stars (LBVs), which do not fully destroy the progenitor star and are therefore not classed as true SNe (e.g. van Dyk et al. 2000; Maund et al. 2006). Four such objects were found in our sample, and the results on these ‘impostors’ are presented and discussed separately in the following sections.

Through the above telescope time allocations we obtained data on host galaxies of a large fraction of the discovered CC SNe that have been classified as IIP, IIL, I Ib, IIn, Ib, and Ic, and were observable within the $H\alpha$ filters of the two telescopes.

There are obvious biases within a set of data chosen in the above way. As we use any discovered SNe for our sample, the various different biases in the different SN surveys that discovered them mean that the galaxy/SN sample is by no means representative of the overall SN populations. Bright, well studied galaxies will be over represented, as will brighter SNe events that are more easily detectable. However, firstly we are not analysing the overall host galaxy properties, but are analysing where within the distribution of stellar populations of the host galaxy the SNe are occurring. Secondly, the small number of SNe of each of the CC sub-types that have been discovered means that no individual survey can currently manage to analyse the properties of their host galaxies or parent stellar populations in any statistically significant way (most statistical observational studies do not even attempt to separate the Ib and Ic SN types). Taking our approach enables us to make statistical constraints on all the major SN types. The results that are presented in this paper are on the analysis of the parent stellar populations of 115 SNI, of which 35 are IIP, 6 IIL, 8 I Ib and 12 IIn, 4 SN ‘impostors’, plus 22 Ib, 30 Ic and 6 that only have Ib/c as their classification, taken from both the initial $H\alpha$ GS sample and our additional data described above. The results for individual SNe obtained from the following analysis are listed in Table A1, together with host galaxy characteristics.

For each SN host galaxy we obtained $H\alpha$ + $[NII]$ narrow band imaging, plus R -band imaging. Standard data reduction (flat-fields, bias subtraction etc) were achieved through the automated pipeline of the LT (Steele et al. 2004), and the INT data were processed through the INT Wide Field Camera (WFC), Cambridge Astronomical Survey Unit (CASU) reduction pipeline. Continuum subtraction was then achieved by scaling the broad-band image fluxes to those of the $H\alpha$ images using stars matched on each image, and subtracting the broad-band images from the $H\alpha$

images. Our reduction made use of various *Starlink* packages.

3 RADIAL APERTURE ANALYSIS

To analyse where within the radial distribution of R -band and $H\alpha$ light SNe occurred, radial growth curves for both were constructed for the host galaxy images. These were derived in the following way. For both the R -band and $H\alpha$ images all apertures were centred on the R -band galaxy centroid positions. Galaxy parameters (semi-major and -minor axis sizes, plus position angles) were taken from the NASA/IPAC Extragalactic Database (NED)³. For face-on spiral and irregular galaxies circular apertures were produced, while for inclined spirals elliptical apertures were produced using the ratio of the galaxy axes taken from NED. These were then checked on each host galaxy image by eye to ensure they were a good fit to the sample images. Concentric apertures were then produced that increased in semi-major axis by $5''$ and sampled the galaxy light out to sky levels. In general 20 to 100 apertures were required to sample the full extent of the galaxy light. For those galaxies where less than 25 apertures were required (43 host galaxies) concentric apertures that increased by $2.5''$ in semi-major axis were used so that a significant sampling of radial positions was achieved. These concentric apertures were then used to produce radial growth curves for each SN host galaxy by calculating the flux within each ellipse of increasing size. This enables one to define the edge of the host galaxy at the point where the curves flatten off as the aperture counts have reached sky levels.

The next step was to calculate the total flux within the aperture just including the SN position. This aperture was calculated using the SN coordinates relative to the galaxy centre, plus both the position and inclination angles of the host galaxy (the value calculated is therefore the semi-major axis of the ellipse that just includes the SN position, taking into account the projection along the minor axis). Using these apertures one can then calculate the fraction of the total galaxy R -band light and $H\alpha$ emission (F_{RR} and $F_{RH\alpha}$ as they will be referred to in the results) that is within the position of each SN. This is achieved by measuring the flux within the SN-containing ellipse and dividing this by the measured flux within the largest ellipse (i.e. the total galaxy flux). In Figure 1 we show an example of this technique at work, where two R -band images of the SN host galaxy NGC 3627 are presented. The top image shows the position of the SNIIP 1973R and the aperture that just includes the SN, while the bottom image has overlaid the aperture that contains all of the R -band flux of the galaxy.

During this analysis it was found that there were some SNe where it was not possible to perform the above procedure accurately. Some of the R -band images were not used due to there being too many bright stars in the field as it can be difficult to remove stars from images without leaving residuals that may affect the results. This in general is not a problem for the $H\alpha$ images as stars are removed through the continuum subtraction applied. There were also images where due to the size of the field of view of the detector used (mainly LT images), it was not possible to apply the radial analysis out the full size of the host galaxies and therefore these data were removed from the subsequent analysis and results.

The method described above normalises the distributions to

² <http://web.pd.astro.it/supern/>

³ <http://nedwww.ipac.caltech.edu/>

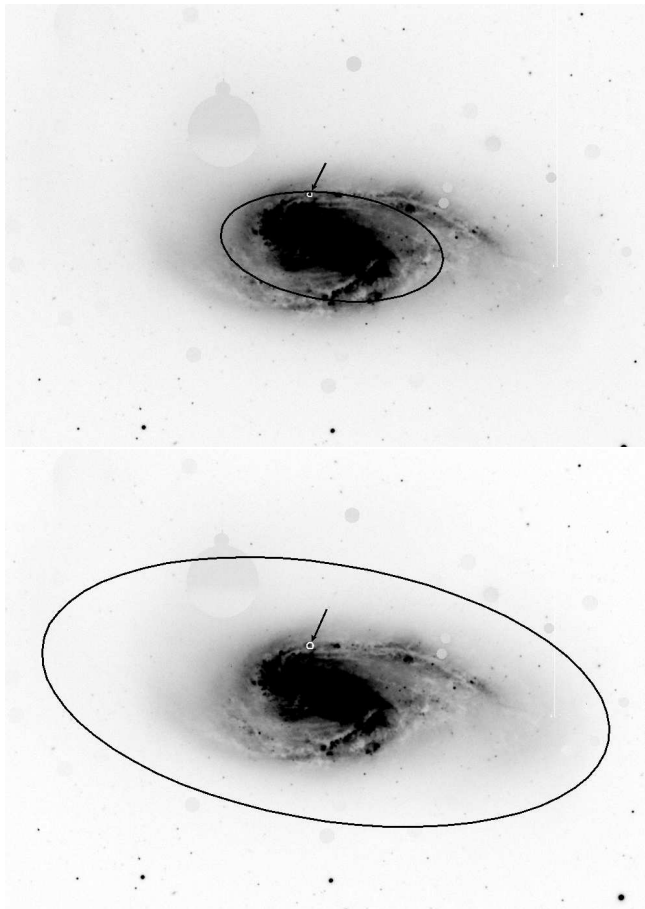


Figure 1. An example of the radial aperture analysis applied to NGC 3627, the host galaxy of the IIP SN 1973R. The top image shows a negative R -band image of the galaxy with the position of the SN indicated by the circle and the arrow, and an aperture overlaid that just includes the SN. The bottom image shows the same galaxy with an aperture overlaid that contains all the flux of the galaxy. The fraction of R -band light within the position of SN 1973R is 0.471.

the host galaxy properties (overall R -band light and $H\alpha$ emission fluxes). This enables an analysis of a sample of SNe that occur in a wide range of galaxy morphologies and sizes, without the characteristics of those host galaxies affecting the overall distribution of SN positions. If one were to merely use absolute SN distance from its host galaxy centre (in say, kpc) then there would be a systematic overabundance of SNe occurring at small radial positions as these positions would be populated with SNe exploding in all host galaxies, while larger radial positions would only be populated by SNe occurring in the largest host galaxies. This normalisation also allows an investigation into whether the different SN types trace the overall distributions of the two types of light within their host galaxies, as discussed in § 1.2.

If the SNe are equally likely to arise from any part of the $H\alpha$ emission or R -band light distributions then one would expect a mean fraction of 0.5 and the fractions of light to be evenly distributed throughout the radial light profiles (i.e. a flat distribution). This is the test that is presented in the following section; whether the different SN types better trace the radial distribution of the R -band light or the $H\alpha$ emission. It is also investigated whether there are differences between the radial distributions of the different SN types and

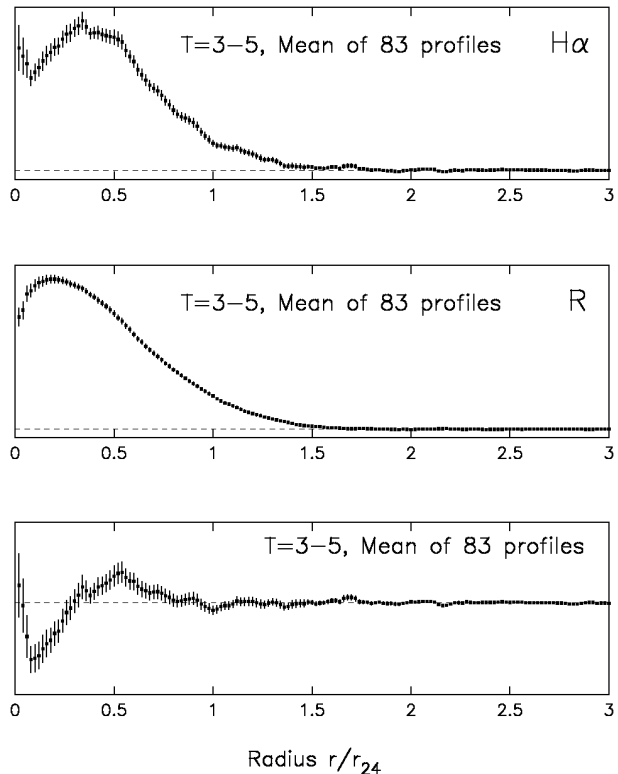


Figure 2. Normalised light profiles for all the $H\alpha$ GS galaxies of types Sb, Sbc, and Sc (83 in total, figures modified from those in James et al. 2009). The top panel shows the radial $H\alpha$ profile averaged over the sample and the middle panel shows the R -band profile. In the bottom panel we show the difference between the mean $H\alpha$ and R -band profiles.

what implications these may have for the nature of their progenitors.

In Fig. 2 we show the normalised radial light profiles (flux in elliptical annuli), averaged over all of the T-types 3-5 galaxies (Sb, Sbc and Sc Hubble types, both barred and unbarred) within the $H\alpha$ GS survey. This range of types is chosen to illustrate the typical light profiles for galaxies used in the present investigation, as they represent those galaxies that dominate the SF within the local Universe (James et al. 2008), and also dominate the morphological types within our sample (as shown in § 5.5). In the top panel we show the averaged $H\alpha$ profile, in the middle panel we show the averaged R -band profile, and finally in the bottom panel we show the difference between the two. In the final plot the central spike is possibly due to central SF or AGN in barred galaxies, while the negative values between r/r_{24} of 0.1 and 0.3 show the effect of the central bulge, where there is a deficit in the SF relative to the R -band light. For a detailed discussion of the calculation of these profiles, and in particular the scaling of the input profiles by radius and total flux, see James et al. (2009).

4 RESULTS

4.1 SNI

The mean fraction of R -band light (F_{R} henceforth) within the positions of the 113 SNI is 0.566 (standard error on the mean of 0.022) while for the $H\alpha$ emission ($F_{H\alpha}$ henceforth) it is 0.572 (0.025). Histograms of these two distributions are shown in Figs. 3 and 4

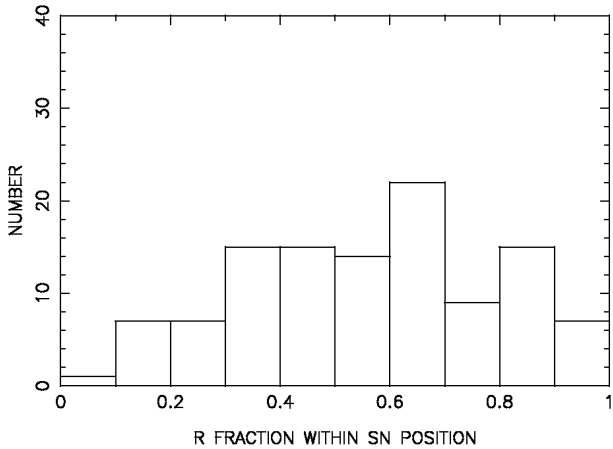


Figure 3. Histogram of the fractional R -band fluxes within the locations of 113 SNIi

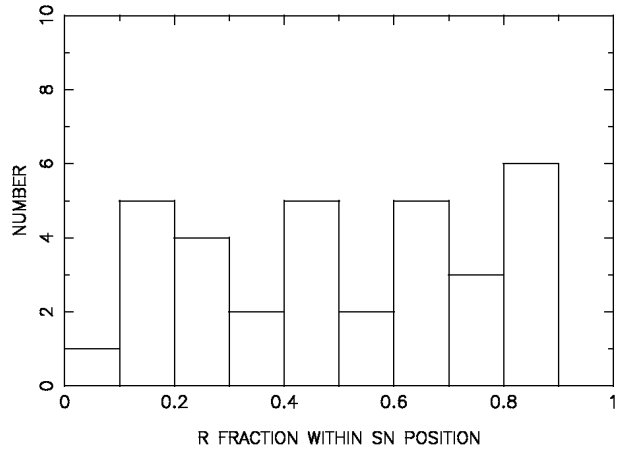


Figure 5. Histogram of the fractional R -band fluxes within the locations of 34 SNIIP

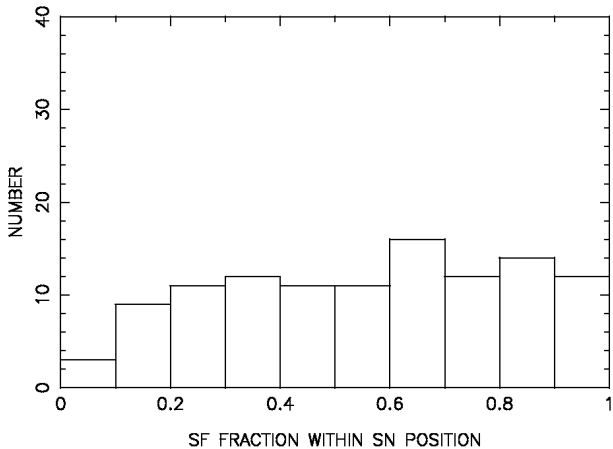


Figure 4. Histogram of the fractional $H\alpha$ fluxes within the locations of 113 SNIi

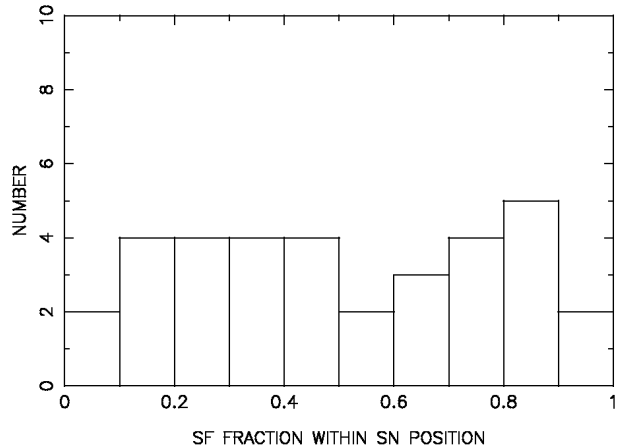


Figure 6. Histogram of the fractional $H\alpha$ fluxes within the locations of 35 SNIIP

respectively. Using a Kolmogorov Smirnov (KS) test there is only $\sim 0.1\%$ chance that the SNIi are drawn from the same radial distribution as the R -band light and there seems to be a deficit at both small and large radii. Although the distribution of SNIi compared to the $H\alpha$ emission appears reasonably flat in Fig. 4, there is only a 5% chance that they follow radial distribution of the HII regions. This is due to the deficit of SNe at small radii which will be discussed in the next section. Results on the individual SNIi sub-types will now be presented.

4.1.1 SNIIP

The $F_{R,R}$ and $F_{R,H\alpha}$ distributions for the SNIIP are shown in Figs. 5 and 6 respectively. Both of these distributions appear similar and are consistent with the SNIIP being drawn from the same population as both the R -band and $H\alpha$ emission (using a KS test), although there appears to be slightly more of a deficit at small and large radii for the SNe with respect to the R -band light, as seen for the overall SNIi population. The mean $F_{R,R}$ is 0.511 (0.046) and the mean $F_{R,H\alpha}$ is 0.522 (0.050). Both of these distributions are also consistent with being drawn from the same population as the overall SNIi values.

4.1.2 Other SNIi sub-types

In Table 1 we list the radial statistics for the SN types IIL, Iib, IIn and ‘impostors’. All these distributions are consistent with being drawn from the same parent population as the overall SNIi. However, we note that all distributions are shifted to higher mean values than the SNIi. The ‘impostors’ in particular seem to be located towards the outer parts of their host galaxies.

SN type	N	$\bar{F}_{R,R}$	σ_M	$\bar{F}_{R,H\alpha}$	σ_M
IIL	6	0.520	0.074	0.561	0.101
Iib	8	0.581	0.106	0.577	0.116
IIn	12	0.591	0.060	0.580	0.089
‘impostors’	4	0.725	0.150	0.757	0.168

Table 1. Radial statistics for the SN sub-types; types IIL, Iib, IIn and ‘impostors’. In the first two columns the SN type and number of events in the sample are given. In columns 3 and 4 the mean $F_{R,R}$ and its associated error are listed followed by the statistics for the $F_{R,H\alpha}$.

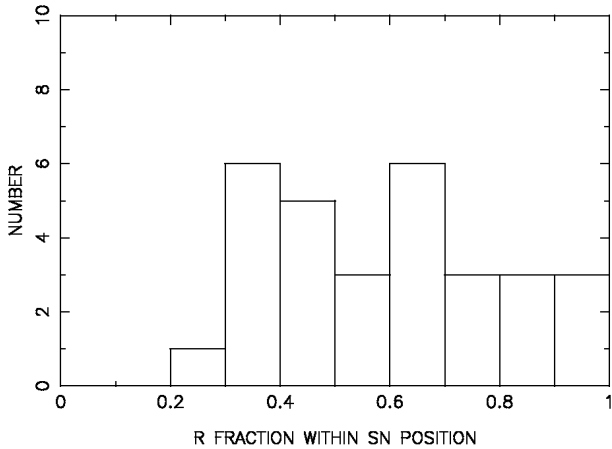


Figure 7. Histogram of the fractional R -band fluxes within the locations of the combined sample of SNIIL, I Ib, I In and SN ‘impostors’ (30 objects in total).

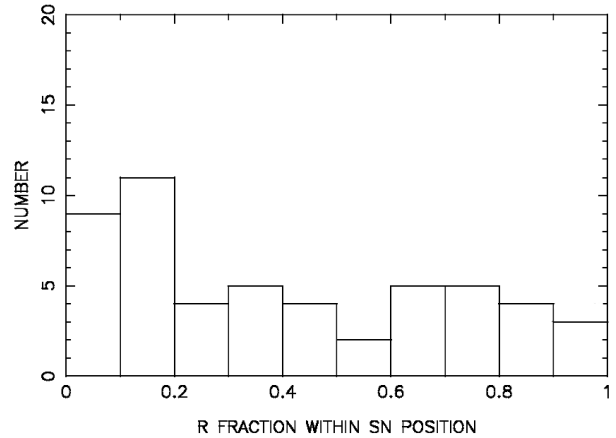


Figure 9. Histogram of the fractional R -band fluxes within the locations of 52 SNIb/c

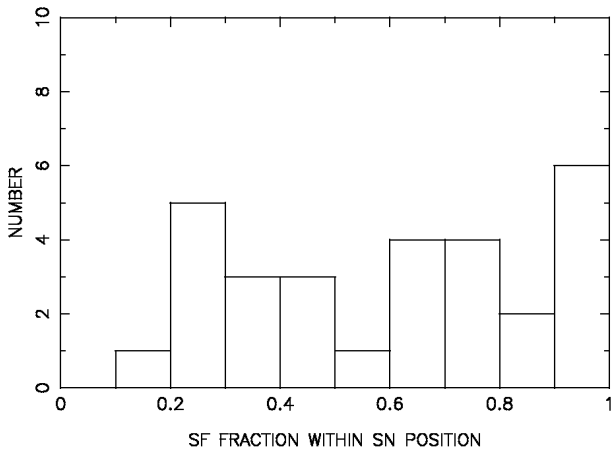


Figure 8. Histogram of the fractional $H\alpha$ fluxes within the locations of the combined sample of SNIIL, I Ib, I In and SN ‘impostors’ (29 objects in total).

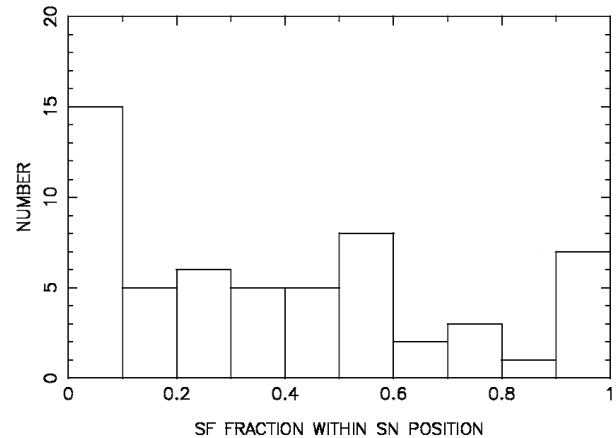


Figure 10. Histogram of the fractional $H\alpha$ fluxes within the locations of 58 SNIb/c

4.1.3 Comparison of SNIIP to other sub-types

For a comparison of the SNI sub-types with the individual SNIIP presented above, in Figs. 7 and 8 the distributions of the combined sample of the SNIIL, I Ib and the I In plus the four SN ‘impostors’ are presented. It is immediately clear that there is a large deficit of these non-IIP SNe at small radii compared to the SNIIP (see Figs. 5 and 6), an effect that seems more prominent in the R -band. However, using a KS test both of the distributions are consistent with those of the SNIIP. The non-IIP SNe have a $\sim 3\%$ chance of being drawn from the distribution of R -band light (i.e. a flat distribution) while they are consistent with being drawn from the $H\alpha$ emission distribution. The mean F_{R} for the 30 non-IIP SNe is 0.592 (0.040) and the mean $F_{H\alpha}$ (only 29) is 0.600 (0.050)

4.2 SNIb/c

The radial distributions of the overall SNIb/c population with respect to the R -band light and $H\alpha$ emission are shown in Figs. 9 and 10 respectively (52 SNe in the R -band histogram and 58 in the $H\alpha$ plot). It is immediately clear that they are weighted to the central parts of the light distribution, especially when comparing them to the other SN types discussed above. This is also reflected

in the mean values of their distributions; the mean F_{R} is 0.408 (0.041) and mean $F_{H\alpha}$ is 0.405 (0.041). Comparing these distributions to that of the overall SNI population it is found that for both the R -band and the $H\alpha$ there is only $\sim 0.1\%$ chance that the SNIb/c and SNI are drawn from the same radial distributions. Comparing the above samples to flat distributions it is found that there is only $\sim 2\%$ chance that the SNIb/c are drawn from the same radial distribution as that of the SF while there is only $\sim 1\%$ chance that they are drawn from the radial distribution of the R -band light. Results on the SNIb and Ic will now be presented separately.

4.2.1 SNIb

The mean F_{R} for the 17 SNIb is 0.468 (0.088) and the mean $F_{H\alpha}$ (22 SNe) is 0.465 (0.072) and histograms of the two distributions are presented in Figs. 11 and 12 respectively. These SNe are consistent with being drawn from the same radial distribution as that of the R -band light and the $H\alpha$ emission of their host galaxies. There is only a $\sim 2\%$ (R -band) and $\sim 7\%$ ($H\alpha$) chance that the SNIb are drawn from the same radial distributions as the SNI.

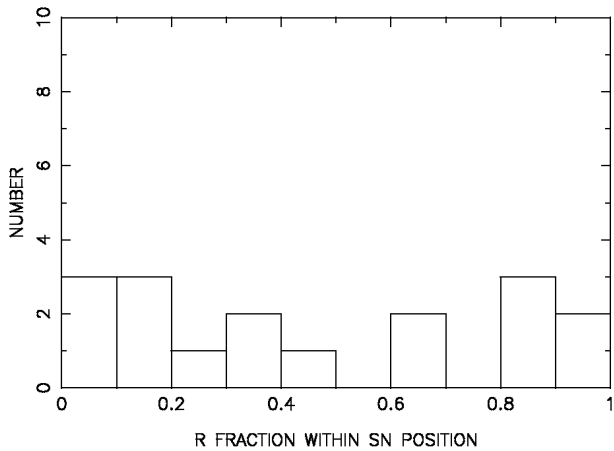


Figure 11. Histogram of the fractional R -band fluxes within the locations of 17 SNIb

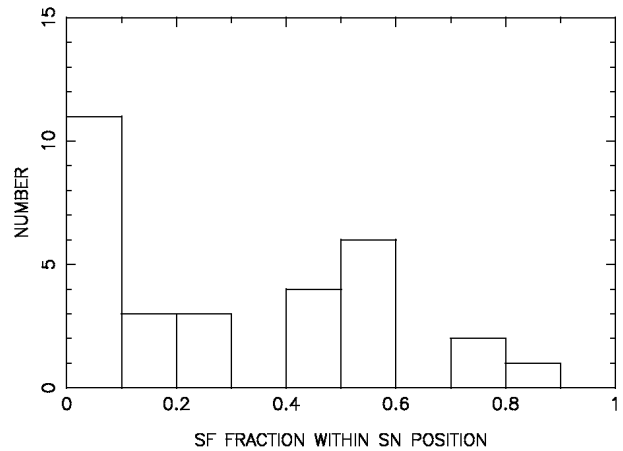


Figure 14. Histogram of the fractional $H\alpha$ fluxes within the locations of 30 SNIc

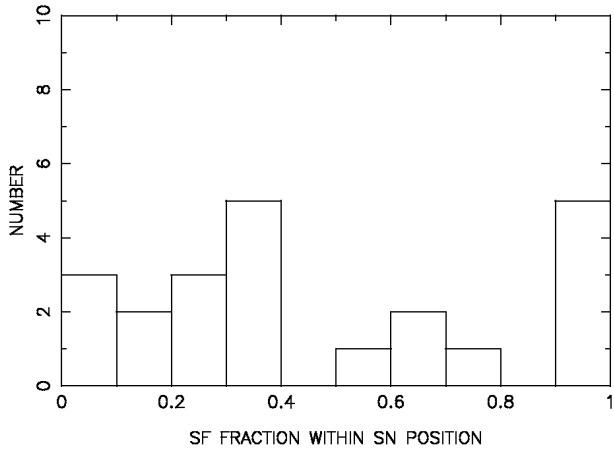


Figure 12. Histogram of the fractional $H\alpha$ fluxes within the locations of 22 SNIb

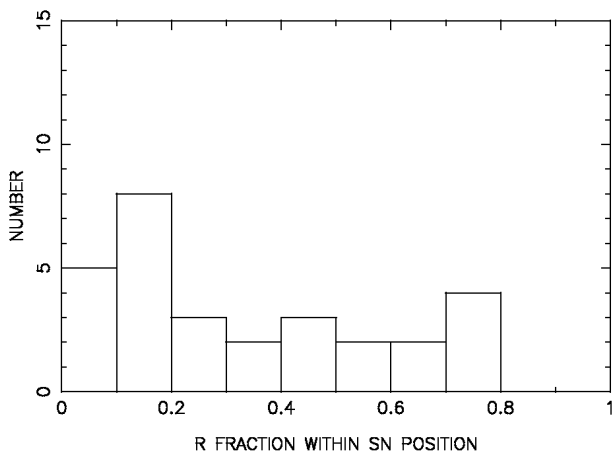


Figure 13. Histogram of the fractional R -band fluxes within the locations of 29 SNIc

4.2.2 SNIc

The Fr_R (29 SNe) and $Fr_{H\alpha}$ (30) distributions for the SNIc are shown in Figs. 13 and 14 respectively. The mean Fr_R is 0.338 (0.047) and the mean $Fr_{H\alpha}$ is 0.306 (0.047). The histograms show that both these distributions are strongly weighted to small light fractions; i.e. the central parts of the light distributions of host galaxies. This is backed up by KS tests that show there is only $\sim 1\%$ chance that the SNIc follow the same radial distributions as that of the R -band light, while there is $< 1\%$ chance that they follow the same radial distribution as the line emission. Comparing these distributions to those of the SNIb it is found that while when looking at their distributions (specifically comparing Figs. 12 and 14, and the mean $Fr_{H\alpha}$ values) they seem to occur at different host galaxy radii (particularly with respect to the complete deficit of SNIc in the outer 20% of the R band light distribution), statistically they are consistent with being drawn from the same parent distribution.

5 DISCUSSION

5.1 Implications for progenitor metallicity

As discussed in § 1.2, radial position within galaxies can be used as a proxy for environment metallicity with galaxy centres tending to have higher metal content. Differences in the radial distributions of SN types can therefore be used to infer differences in progenitor metallicity. Comparing Fig. 9 to Fig. 3 it is immediately clear that the SNIb/c are more centrally concentrated than the SNIc (a result also seen in van den Bergh 1997, and most recently Hakobyan 2008) implying higher metallicity progenitors. This trend is also backed up by the KS statistics presented above. To further illustrate this point, in Fig. 15 the cumulative distributions of the radial positions of the main CC SN types (II, Ib and Ic) with respect to the R -band light are plotted (the R -band light distribution is chosen to show this result as it will be a more reliable indicator of integrated SF over the galaxy's lifetime, and therefore metallicity, than the distribution of $H\alpha$ emission). Apart from a central deficit of SNIc these SNe seem to follow the distribution of R -band light while the SNIb then the SNIc appear more centrally concentrated as their distributions are biased to smaller radii. This plot implies that the SNIb/c tend to preferentially occur in regions of higher metallicity than SNIc. The arrow on the plot shows the implied direction

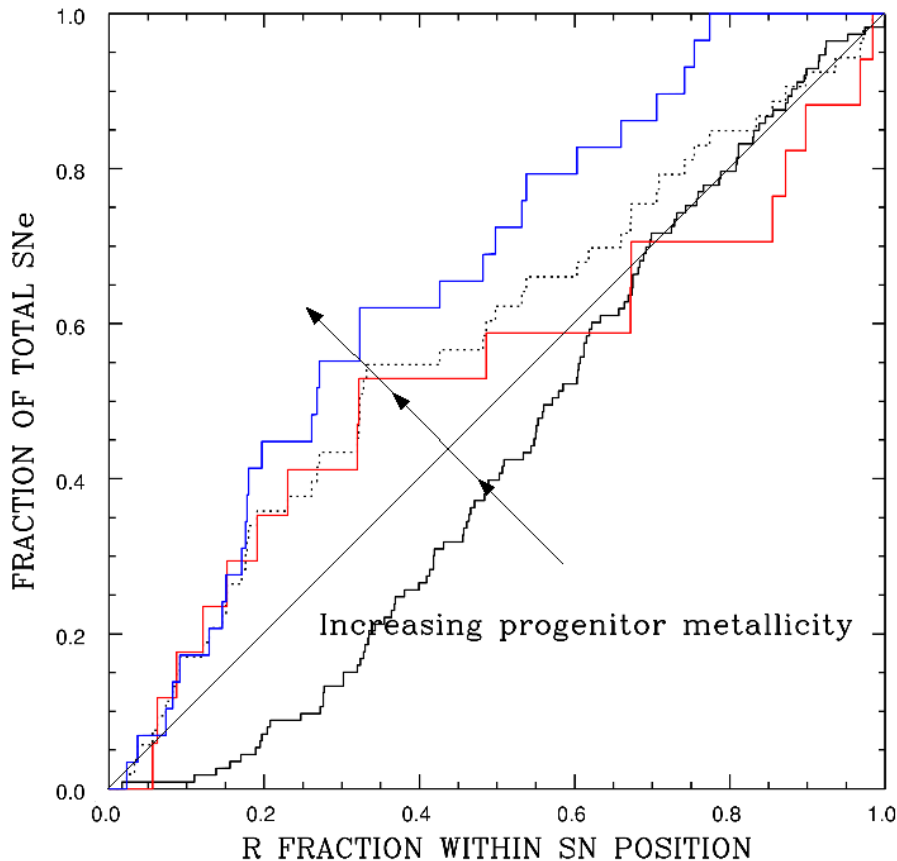


Figure 15. Plot showing the cumulative distributions of the radial positions of the main CC SN types with respect to the R -band light of their host galaxies. The SNII distribution is plotted in black, the SNIIb in red, the SNIIc distribution is blue and the overall SNIIb/c population in dotted black. There is also a hypothetical flat distribution (i.e. one that accurately traces the radial distribution of R -band light) plotted as a diagonal black line.

of increasing metallicity and one can see that a trend is observed going from SNII to SNIIb and finally SNIIc arising from progenitors of the highest metallicity. Stars of higher metallicity tend to have stronger radiatively driven stellar winds (e.g. Puls et al. 1996; Kudritzki & Puls 2000; Mokiem et al. 2007). As discussed in § 1.1 the spectral appearance of SNIIb suggests that these SNe have lost their hydrogen envelopes while SNIIc spectra indicate that they have also lost their helium envelopes. The results presented above are therefore consistent with progenitor metallicity playing a significant role in removing SN progenitor envelopes and producing the different CC SNe that we see.

This metallicity dependence has also been seen in research looking at the host galaxy properties of CC SNe. Prantzos & Boissier (2003) looked at the relative rates of SNII and SNIIb/c as a function of host galaxy luminosity, using this as a proxy for metallicity. They found that the ratio of SNII to SNIIb/c events strongly correlated with host luminosity in the sense that relatively more SNIIb/c were found in more luminous, i.e. more metal rich environments. Prieto et al. (2008) investigated the metallicity of SDSS galaxies that had hosted CC SNe using spectra and came to similar conclusions. While our results are consistent with these findings, they would also suggest that the metallicity implications that these authors discuss are underestimates of the true differences between progenitor metallicity of SNIIb/c and SNII (as Prieto et al. 2008 point out). This is due to the fact that while SNIIb/c seem to arise from higher metallicity host galaxies, they are also more

centrally concentrated, and therefore within these host galaxies are likely to come from higher metallicity stellar populations than SNII as well. These different studies (including the current analysis) are also consistent with the model predictions of single stellar models (e.g. Heger et al. 2003, Eldridge & Tout 2004), that SNIIb/c generally arise from more metal rich progenitors. One point that we emphasise here is that these studies (and others), plus stellar models tend to group SNIIb and SNIIc together when discussing differences in progenitor characteristics. We find that when splitting these SNe into their Ib and Ic classifications there appears to be a trend in progenitor characteristics that we observe, implied from the results presented both here and in AJ08. This trend implies that SNIIb tend to arise from higher mass and more metal rich progenitors than SNII, while SNIIc arise from still higher mass and metallicity progenitors.

We note that while the statistics that we present here, plus those from elsewhere suggest that *on average* SNIIc arise from metal rich stellar populations, a number of cases that do not fit this trend have been observed. Examples of these can be found in Modjaz et al. (2008) and Prieto et al. (2008). Therefore while SNIIc seem to favour high metallicity environments, it seems that these events can arise from low metallicity progenitors.

5.2 Comparison of SN and stellar radial distributions

Although the overall SNII population follows the distribution of SF as indicated in Fig. 4 (as would be expected for SNe with massive progenitors), there is a substantial deficit at small radii, a result that was also seen in JA06. One may initially presume that this is due to the bulge components of galaxies within their centres that are too old to produce SNII. However, this distribution is *with respect to the SF of the host galaxies* and therefore there *is* a fraction of high mass SF (the central tenth of the emission) that is not producing its share of SNII. One possible explanation is the decreasing efficiency of detecting SNe in the central parts of galaxies due to either the high surface brightness of the stellar background (Shaw 1979) or extinction effects which have been deduced to result in significant deficits in SN detection rates, even in near-IR searches (Mannucci et al. 2003). Another explanation is that there is an additional emission-line component at the centres of galaxies that is not related to SF and hence not linked to SNII. However, both of these explanations would then seem in contradiction to the above findings that SNIb/c are *more* centrally concentrated than would be expected if they accurately traced the emission, which is also seen with respect to the *R*-band light (see Figs. 9 and 10), as there seems no reason why these effects would apply to the SNII but not the SNIb/c (although the possible effects of differences in intrinsic SN brightness will be discussed below). If one then follows the above arguments on radial positions being indicators of metallicity of stellar environment, this then implies that there is some metallicity upper limit, above which SNII tend not to occur in significant numbers. The stellar models of Eldridge & Tout (2004) predict that the minimum initial mass for producing SNII increases with metallicity. Therefore the increased metallicity in galaxy centres may be expected to produce a smaller fraction of SNII than in the lower metallicity outer disk regions (although note that the models of Heger et al. 2003, do not predict a change in the minimum initial mass). Therefore the most plausible explanation for the above result seems to be that there is some physical mechanism that favours the production of SNIb/c and also limits the production of SNII in the centres of galaxies.

A remarkable feature of Fig. 13 is that 13 out of the 29 SNIc arise from the central 20% of the *R*-band luminosity of these galaxies, which would generally be assumed to be dominated by the passive, non-star forming bulge population.

5.3 The overall CC SN distribution and correlations with host galaxy star formation

In Fig. 16 we show the distributions of locations of all types of CC SNe combined, together with the individual SNII distribution to show the relative contribution of the different SN types at different radii, with respect to the distribution of host galaxy $H\alpha$ emission. This distribution is remarkably flat and consistent with the CC SNe being drawn from the same stellar population as that of the recent SF, and the mean $Fr_{H\alpha}$ is 0.516 (0.023). We can therefore conclude that the $H\alpha$ emission within galaxies accurately traces the CC SN progenitor parent stellar population, and this further implies that both CC SNe and $H\alpha$ emission are excellent tracers of SF within galaxies. This plot then implies that (as discussed above) the central deficit of SNII (and the central excess of SNIb/c) is due to higher metallicities resulting in relatively more SNIb/c than SNII, while as one goes further out into the disk of galaxies the lower metallicities inhibit the production of SNIb/c relative to SNII.

Another explanation for the above results is that there are deviations from a 'normal' IMF as a function of radial positions. Maness et al. (2007) investigated the properties of 329 late-type giant stars in the central parts of the Galaxy. They concluded that these stars originated from a top-heavy IMF. If this applies to the current sample then the above results can be explained by relatively more high mass stars being formed and hence fractionally more progenitor stars exploding as SNIb/c than as SNII when compared to the outer parts of galaxies with standard IMF stellar populations. However, this would not naturally produce the flat distribution seen in Fig. 16 (in fact, the higher fraction of high mass stars would give more central $H\alpha$ emission per SN progenitor star).

It can be asked whether the fraction of different events within the current sample is a true reflection of reality as the sample was not chosen to be complete. However when the make up of the sample is compared to recent local estimates of the relative SN rates (e.g. Smartt et al. 2009), good agreement is found (the only real discrepancy is the additional numbers of the SNIIL, I Ib and I In at the expense of SNIIP). The percentages of SNII and SNIb/c in the current sample are 66% and 34% respectively compared to the Smartt et al. estimates of 71% and 29%.

The different CC SNe discussed above have different characteristic absolute magnitudes. This could therefore affect their relative detections at different radial positions (e.g. there may be more extinction or a higher stellar background in central regions). Richardson et al. (2002) used the Padova-Asiago SN catalogue to carry out a comparative study of SN absolute magnitude distributions. They determined mean peak absolute magnitudes in the *B*-band of -18.04 for SNIb/c, -17.00 for SNIIP, -18.03 for SNIIL and finally -19.15 for SNIIn. One may speculate that the fainter magnitudes of SNIIP (the most abundant SNII sub-type) compared to the SNIb/c naturally explains the higher fraction of SNIb/c in the centres of galaxies where there is likely to be higher extinction and a higher stellar background, preventing the detection of lower luminosity events (however the SNIIP have a plateau phase in their light curves after maximum light meaning that they will be detectable over a longer time period). It is possible that these selection effects could affect the above results, however this effect would have to be quite severe and it is interesting to note that there are no SNIIn (out of 12 in the current sample), the brightest CC SNe according to Richardson et al. (2002), detected within the central 20% of the SF or the central 30% of the *R*-band light.

It is stressed here that while there are many processes that may be at play in producing more or less of the different CC SNe at different radii, nearly all those discussed above would not produce a flat distribution as is seen in Fig. 16. The only interpretation of these results that naturally produces the extremely flat distribution observed, is that CC SNe are produced from a constant mass range of stars that have a non-changing IMF, and that the change in relative numbers of SNII and SNIb/c seen in the centres of galaxies is down to there being a substantial metallicity dependence of progenitors. Within the central 10% of the SF within host galaxies more SNIb/c than SNII have been produced within the current sample.

5.4 SNII sub-types

In § 4.1.3 the distributions of the SNIIP were compared to those of all the other SNII sub-types and the SN 'impostors' (the small number of SNe of each of the other sub-types meant that a statistical comparison of each individually was not viable). It can be seen

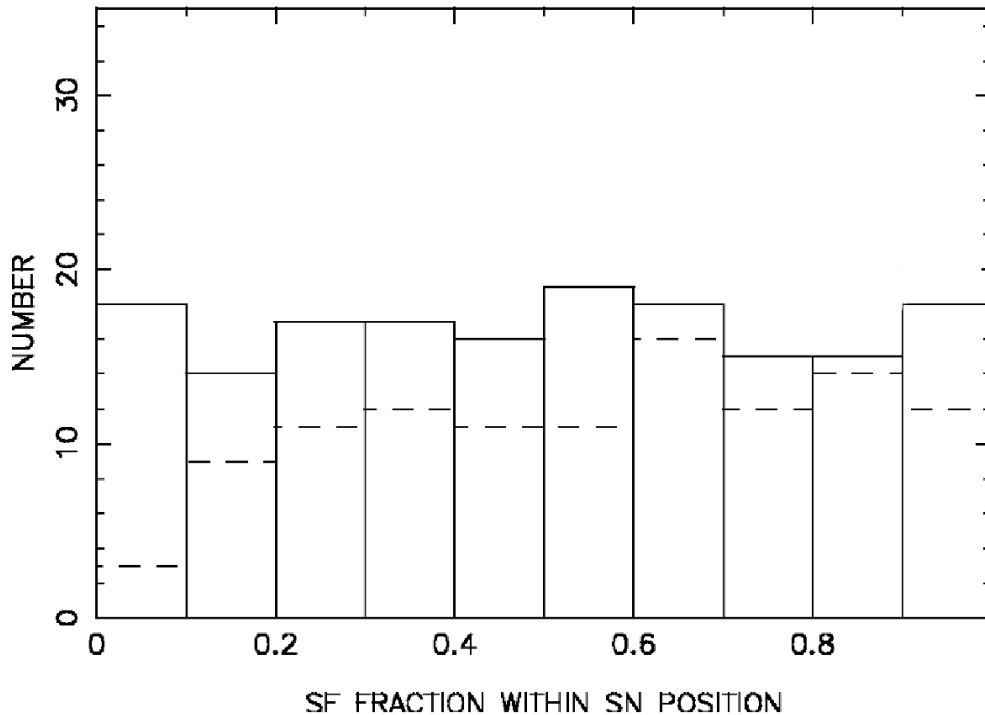


Figure 16. Histogram of the fractional $H\alpha$ fluxes within the locations of the overall CC SN population. The overall CC population are plotted in the solid histogram while the SNIIs are plotted as the dashed histogram.

that all the other sub-types tend to preferentially occur at larger radii with respect to both the R -band light and the $H\alpha$ emission (see Figs. 5, 6, 7 and 8 plus the mean values given for the various types in § 4). While there only seems a slight deficit in SNIIP at small radii with respect to the R -band light, there is only one SN of the other types that has exploded within the inner 30% of the light (this difference is also seen with respect to the $H\alpha$ emission, but to a lesser extent). Again if we regard these differences in terms of radial metallicity gradients within host galaxies then one comes to the conclusion that SNIIP arise from more metal rich progenitors than the other sub-types. However, the spectra of the SNIIs sub-types indicate that their progenitors can be sorted into a sequence of increasing pre-SN stellar mass-loss going from SNIIP to IIL, I Ib and finally IIn (Chevalier 2006). Therefore if there was a metallicity dependence on producing the SNIIP compared to the other sub-types one would presume that in fact SNIIP would be found in less metal rich environments than those of the SNIIL, I Ib, IIn and SN ‘impostors’ (higher metallicity progenitors are likely to have stronger stellar winds). Theory also predicts that SNIIL and I Ib will only be produced above some limiting metallicity (Heger et al. 2003). While these differences between SNIIs sub-type environments are not statistically significant, it is clear that there is some process that is preventing SNIIL, I Ib, IIn and SN ‘impostors’ from being detected or occurring within the central parts of galaxies. The selection effects that may be at play to reduce the detections of these events in the central regions of galaxies were discussed in the previous section, and while these may seem valid by themselves the detection of large numbers of SNIb/c in the same central regions again makes these explanations unsatisfactory. The most plausible explanation seems therefore to be that there is some higher metallicity limit that inhibits the production of these SNe.

5.5 Morphological classifications of SN host galaxies

One may question whether there are intrinsic differences between the host galaxies of the different SN types that may influence our results. To investigate this possibility morphological classifications were taken from the Padova-Asiago SN catalogue for each SN host galaxy in the current sample. There were 9 galaxies within our sample for which classifications were not available. For these we used our own R -band imaging to assign morphological types. All host galaxy classifications were then changed to T-type classifications following the prescription in de Vaucouleurs (1959). The sample was then split into SNI, SNIb and SNIc host galaxies. Mean T-types were found of; 4.60 (standard error on the mean of 0.18) for the SNI, 4.73 (0.39) for SNIb and 4.45 (0.37) for SNIc, and using a KS test it was found that all three galaxy distributions were consistent with being drawn from the same parent population. It therefore seems that there are no significant differences in host galaxy characteristics that could strongly bias the results presented above. It is interesting to note that the distribution of T-type classifications for the galaxies in the current sample peaks between Sbc and Sc galaxies, consistent with the findings of James et al. (2008), that the SFR in the local universe is concentrated within these galaxy types.

5.6 The radial distribution of SNe with respect to host galaxy D_{25} and the nature of galaxy metallicity gradients

The analysis above was based on fractions of total galaxy fluxes lying within SN locations. However, metallicity gradients in galaxies are usually quoted as logarithmic changes over a radial range normalised to an isophotal galaxy size, e.g. dex per (r/D_{25}) . Therefore, here we present a further analysis using r/D_{25} in place of fractional

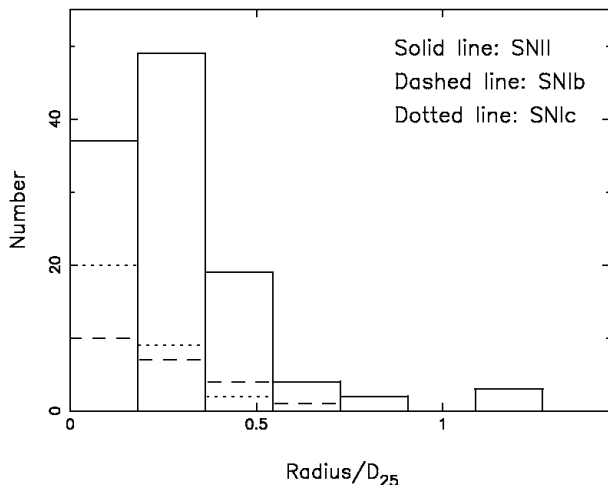


Figure 17. Histogram of the galactocentric radial positions of the different CC SNe types normalised to their host galaxy D_{25} isophotal diameters. The solid line shows the distribution of SNII, dashed line the SNIb, and the dotted line the SNIc

luminosity. We do this to a) check the robustness of the above results and discussion, and b) to make some quantitative statements on the differences in metallicity of the host stellar environments of CC SNe.

For the complete SN and host galaxy sample discussed above we used the radius of the semi-major axis (in arcsec) of the aperture that just includes the SN position (calculated in § 3) and normalise this by dividing by the D_{25} semi-major axis of the host galaxy taken from NED, giving a value of r/D_{25} . The distribution of these values for the SNII, SNIb and SNIc populations is shown in Fig. 17. This plot shows qualitatively the same results as shown in the histograms presented in § 4 and the cumulative distribution plot shown in Fig. 15. The SNIc are the most centrally concentrated distribution, followed by the SNIb and the SNII, implying, as above, a decreasing sequence of progenitor metallicity. The mean r/D_{25} for the SNIc is 0.149 (standard error on the mean of 0.024), 0.244 (0.032) for the SNIb and 0.295 (0.020) for the SNII distribution. Using KS tests we find that there is less than 0.1% probability that the SNIc are drawn from the same radial distribution as that of the SNII, while the SNIb are consistent with arising from the same parent distribution as that of the SNII. There is a 7.7% chance that the SNIb and SNIc distributions arise from the same parent population.

Henry & Worthey (1999) published metallicity gradients for a range of galaxy types. They found a mean metallicity gradient within galaxies of $[O/H] = -1.0(r/D_{25})$ (a value also observed by Prantzos & Boissier 2000). Using this gradient together with the differences between the mean values of r/D_{25} presented above we estimate that the mean metallicity difference between the stellar environments of SNIc and SNII is roughly 0.15 dex, i.e. that SNIc arise from progenitors with metal abundances a factor of 1.4 higher on average than those of SNII.

The above analysis shows that there are real differences in the radial positions of the different CC SN types. However, it is not clear whether the metallicity differences that we derive can alone produce the differences in the relative rates of SNIc and SNII that we find between galaxy centres and out in the disc, and therefore other factors must be at play. As discussed earlier, studies investigating the global host galaxy properties (Prantzos & Boissier

2003; Prieto et al. 2008) have concluded that SNIb/c are generally found in higher metallicity galaxies than SNII. We therefore investigated this in the current sample. Host galaxy absolute B -band magnitudes were calculated using galaxy photometry and distances taken from NED. Surprisingly we do not recover the differences in host galaxy magnitude between the SNIb/c and SNII published by Prantzos & Boissier, and all host galaxy magnitude distributions are statistically the same. It is not clear what is the cause of this discrepancy because, as shown above the host galaxy morphologies in our sample are typical for SF galaxies and therefore one would assume typical for the Prantzos & Boissier sample, which was drawn from the Padova-Asiago SN catalogue. One possibility is that the current sample is too small to observe differences in the host galaxy magnitudes (and we also note the size of the error bars in their analysis). We also note that in interpreting these results, it should be borne in mind that many SNe are detected in searches targeted on bright galaxies, which may somewhat affect the metallicity effects between galaxies, although any effect can only be small.

While Prantzos & Boissier used host galaxy magnitude as a proxy for galaxy metallicity, Prieto et al. (2008) obtained host galaxy metallicities derived from spectra of the host galaxies and again found that SNIb/c were typically found in more metal rich galaxies than SNII. Therefore it seems likely that SNIb/c arise from both more metal rich galaxies and, as found in the current study more metal rich environments within those galaxies. However, we concur with the conclusion of Prieto et al., that metallicities should be directly derived at the SN locations, and we have such a project underway (see also Modjaz et al. 2008, for a similar study).

5.7 Implications for progenitor metallicity or mass?

In this paper we have generally assumed that the increased centralisation of a SN distribution implies increased progenitor metallicity. Recently Kelly et al. (2008) presented statistics on the association of SNe to the g' -band light of their host galaxies (using a similar fractional flux technique as that presented in AJ08), which has been modeled by Raskin et al. (2008) to derive initial progenitor mass estimates. This work showed that SNIc are concentrated towards the brightest parts of their host galaxies while the SNIb and SNII populations followed the distribution of g' -band light. These authors then argue that the brightest regions of galaxies are likely to correspond to the largest SF regions, where the most massive stars are formed, a plausible argument given that SF results in local enhancement of g' -band luminosity. Using this assumption they conclude that SNIc arise from higher mass progenitors than SNII and SNIb. However, this interpretation is ambiguous, since g' -band brightness can be enhanced from other causes, and in particular shows a systematic trend with radius, and hence plausibly with metallicity, which complicates the interpretation of their result.

Our method, presented in AJ08 and the current paper, attempts to disentangle effects due to progenitor mass/age and those due to metallicity. The correlations of AJ08 make use of the continuum-subtracted $H\alpha$ surface brightness, which explicitly traces only the young stellar population, independently of radial position and local metallicity. The present paper demonstrates that, within that very young stellar population, the part laying closest to the galaxy centres tends to produce large numbers of SNIc, and fewer SNII. These radial changes we attribute to metallicity effects.

5.8 Progenitor binarity

One major point of discussion that we have up to this point ignored is the possibility that a large fraction of CC SN progenitors (in particular the SNIb/c) may arise from binary systems. As discussed earlier the relative ratio of SNIb/c to SNII when compared with predictions from single star models and observations of massive stars in the local group (Massey 2003, Crowther 2007), would seem to suggest that the production of a significant fraction of SNIb/c from binaries is required. While a detailed discussion of CC SN production through binaries and how this may be affected by environment is beyond the scope of this paper, here we briefly summarise the points that may be relevant to the current work. As with single stars, theory in general predicts that the production of SNIb/c from binaries should increase with increasing progenitor metallicity (see Fryer et al. 2007 and Eldridge et al. 2008, although also see Izzard et al. 2004 for differing predictions). If correct, the higher degree of centralisation of SNIb/c (and in particular SNIc), can be explained again in terms of increasing metallicity, which increases the relative production of these SNe through both single *and* binary progenitor scenarios. We also note that Eldridge et al. (2008) have shown that the observed trends of the ratio of SNII to SNIb/c with metallicity (they use the SN host galaxy luminosity observations of Prantzos & Boissier 2003) are most convincingly reproduced from binary model predictions. Therefore, while in general we have discussed our results in terms of single star SN progenitors, it seems that the implications of our results are also compatible with current thinking on SN production from binary channels, and further work is needed in order to further constrain the fraction of events produced by the different progenitor scenarios.

6 CONCLUSIONS

We have presented results and discussion on the radial distribution of CC SNe with respect to both old stellar populations as traced by the *R*-band continuum light and young stellar populations as traced by the $H\alpha$ emission within host galaxies. We find that the distribution of the overall CC SN population closely follows the distribution of $H\alpha$ line emission, implying that both are accurate tracers of SF within galaxies. Within this correlation we find that the ratio of SNII to SNIb/c is strongly correlated with galactocentric radial position, with the SNIb/c (in particular the SNIc) dominating the CC SN production within the central parts of the host galaxies' SF while as one moves out into the disk the SNII become more dominant. This implies a strong metallicity dependence on the relative production of these SN types from massive star progenitors. We now list our main conclusions that arise from this work:

- The radial distribution of CC SNe closely follows the radial distribution of $H\alpha$ emission within galaxies with a central deficit in the number of SNII offset by a central excess of SNIb/c. This implies that both CC SNe and $H\alpha$ emission are excellent tracers of SF within galaxies

- SNIb/c are observed to occur within more central positions of host galaxies than SNII implying that they arise from more metal rich progenitors. This confirms and strengthens the results of van den Bergh (1997), Tsvetkov et al. (2004) and Hakobyan (2008)

- SNIc are seen to be the most centrally concentrated of all CC SN types with many SNe occurring within the central 20% of the host galaxy light and none found to occur in the outer 20%. This implies that the majority of SNIc occur within metal rich environments

- SNIb are found to trace the host galaxy light and line emission more accurately than the SNIc while still being more centrally concentrated than the SNII, implying a progenitor metallicity sequence going through SNII, SNIb and SNIc, with the latter arising from the highest metallicity progenitors

- SNIIP are found to be more centrally concentrated than the other SNII sub-types implying that SNe of types SNIIL, IIB, and IIn generally arise from less metal rich progenitors than SNIIP, in apparent contradiction to theoretical predictions

ACKNOWLEDGMENTS

We thank the anonymous referee for their constructive comments. We also thank Stephen Smartt and Mike Bode for useful discussion, and Mike Irwin for processing the INT data through the CASU WFC automated reduction pipeline. This research has made use of the NASA/IPAC Extragalactic Database (NED) which is operated by the Jet Propulsion Laboratory, California Institute of Technology, under contract with the National Aeronautics and Space Administration.

REFERENCES

- Anderson J. P., James P. A., 2008, MNRAS, 390, 1527
 Barbon R., Ciatti F., Rosino L., 1979, A&A, 72, 287
 Bartunov O. S., Makarova I. N., Tsvetkov D. I., 1992, A&A, 264, 428
 Burket J., Pugh H., Li W., Puckett T., Cox L., 2005, IAUC CBET, 8504, 2
 Chevalier R. A., 2006, ArXiv Astrophysics e-prints
 Chugai N. N., Danziger I. J., 1994, MNRAS, 268, 173
 Crowther P. A., 2007, ARA&A, 45, 177
 de Vaucouleurs G., 1959, Handbuch der Physik, 53, 275
 Eldridge J. J., Izzard R. G., Tout C. A., 2008, MNRAS, 384, 1109
 Eldridge J. J., Tout C. A., 2004, MNRAS, 353, 87
 Filippenko A. V., 1993, in Bulletin of the American Astronomical Society Vol. 25 of Bulletin of the American Astronomical Society, The Spectroscopic and Photometric Evolution of Type II Supernovae. pp 819+
 Filippenko A. V., 1997, ARA&A, 35, 309
 Filippenko A. V., Matheson T., Ho L. C., 1993, ApJ Let., 415, L103+
 Fryer C. L., et al., 2007, PASP, 119, 1211
 Ganeshalingam M., Graham J., Pugh H., Li W., 2003, IAUC CBET, 8134, 1
 Gaskell C. M., Cappellaro E., Dinerstein H. L., Garnett D. R., Harkness R. P., Wheeler J. C., 1986, ApJ Let., 306, L77
 Goodrich R. W., Stringfellow G. S., Penrod G. D., Filippenko A. V., 1989, ApJ, 342, 908
 Graham J., Li W., Schwartz M., Trondal O., 2005, IAUC CBET, 8465, 1
 Hakobyan A. A., 2008, Astrophysics, 51, 69
 Hamuy M., 2003, ApJ, 582, 905
 Heger A., Fryer C. L., Woosley S. E., Langer N., Hartmann D. H., 2003, ApJ, 591, 288
 Hendry M. A., et al., 2006, MNRAS, 369, 1303
 Henry R. B. C., Worthey G., 1999, PASP, 111, 919
 Izzard R. G., Ramirez-Ruiz E., Tout C. A., 2004, MNRAS, 348, 1215
 James P. A., Anderson J. P., 2006, A&A, 453, 57

APPENDIX A: SN AND HOST GALAXY DATA

- James P. A., Bretherton C. F., Knapen J. H., 2009, ArXiv e-prints
- James P. A., et al., 2004, *A&A*, 414, 23
- James P. A., Knapen J. H., Shane N. S., Baldry I. K., de Jong R. S., 2008, *A&A*, 482, 507
- Kelly P. L., Kirshner R. P., Pahre M., 2008, *ApJ*, 687, 1201
- Kudritzki R.-P., Puls J., 2000, *ARA&A*, 38, 613
- Maness H., Martins F., Tripp S., Genzel R., Graham J. R., Sheehy C., Salaris M., Gillessen S., Alexander T., Paumard T., Ott T., Abuter R., Eisenhauer F., 2007, *ApJ*, 669, 1024
- Mannucci F., Maiolino R., Cresci G., Della Valle M., Vanzì L., Ghinassi F., Ivanov V. D., Nagar N. M., Alonso-Herrero A., 2003, *A&A*, 401, 519
- Massey P., 2003, *ARA&A*, 41, 15
- Matheson T., Calkins M., 2001, *IAUC CBET*, 7597, 3
- Matheson T., Jha S., Challis P., Kirshner R., Berlind P., 2001, *IAUC CBET*, 7756, 4
- Maund J. R., et al., 2006, *MNRAS*, 369, 390
- Maund J. R., Smartt S. J., Kudritzki R. P., Podsiadlowski P., Gilmore G. F., 2004, *Nature*, 427, 129
- Mazzali P. A., Deng J., Maeda K., Nomoto K., Filippenko A. V., Matheson T., 2004, *ApJ*, 614, 858
- Modjaz M., Kewley L., Kirshner R. P., Stanek K. Z., Challis P., Garnavich P. M., Greene J. E., Kelly P. L., Prieto J. L., 2008, *AJ*, 135, 1136
- Mokiem M. R., et al., 2007, *A&A*, 473, 603
- Nomoto K., Suzuki T., Shigeyama T., Kumagai S., Yamaoka H., Saio H., 1993, *Nature*, 364, 507
- Pastorello A., et al., 2004, *MNRAS*, 347, 74
- Podsiadlowski P., Hsu J. J. L., Joss P. C., Ross R. R., 1993, *Nature*, 364, 509
- Podsiadlowski P., Joss P. C., Rappaport S., 1990, *A&A*, 227, L9
- Prantzos N., Boissier S., 2000, *MNRAS*, 313, 338
- Prantzos N., Boissier S., 2003, *A&A*, 406, 259
- Prieto J. L., Stanek K. Z., Beacom J. F., 2008, *ApJ*, 673, 999
- Pugh H., Li W., Manzini F., Behrend R., 2004, *IAUC CBET*, 8452, 2
- Puls J., et al., 1996, *A&A*, 305, 171
- Raskin C., Scannapieco E., Rhoads J., Della Valle M., 2008, *ApJ*, 689, 358
- Richardson D., Branch D., Casebeer D., Millard J., Thomas R. C., Baron E., 2002, *AJ*, 123, 745
- Schlegel E. M., 1990, *MNRAS*, 244, 269
- Shaw R. L., 1979, *A&A*, 76, 188
- Smartt S. J., Eldridge J. J., Crockett R. M., Maund J. R., 2009, *MNRAS*, 395, 1409
- Steele I. A., et al., 2004, in Oschmann Jr. J. M., ed., *Ground-based Telescopes*. Edited by Oschmann, Jacobus M., Jr. Proceedings of the SPIE, Volume 5489, pp. 679-692 (2004). Vol. 5489 of Presented at the Society of Photo-Optical Instrumentation Engineers (SPIE) Conference, The Liverpool Telescope: performance and first results. pp 679–692
- Tsvetkov D. Y., 1994, *Astronomy Letters*, 20, 374
- Tsvetkov D. Y., Pavlyuk N. N., Bartunov O. S., 2004, *Astronomy Letters*, 30, 729
- van den Bergh S., 1997, *AJ*, 113, 197
- van Dyk S. D., 1992, *AJ*, 103, 1788
- van Dyk S. D., Filippenko A. V., Chornock R., Li W., Challis P. M., 2005, *PASP*, 117, 553
- van Dyk S. D., Peng C. Y., King J. Y., Filippenko A. V., Treffers R. R., Li W., Richmond M. W., 2000, *PASP*, 112, 1532
- Williams K. A., Bolte M., Koester D., 2009, *ApJ*, 693, 355

Table A1. Data for all SNe and host galaxies

SN	SN type	Host galaxy	Galaxy type	V_r (kms $^{-1}$)	Fr_R	$Fr_{H\alpha}$	Filter	Reference
1921B	II	NGC 3184	SABcd	592	0.856	0.954	<i>R</i>	
1926A	III	NGC 4303	SABbc	1566	0.607	0.736	<i>R</i>	
1937F	IIP	NGC 3184	SABcd	592	0.808	0.930	<i>R</i>	
1940B	IIP	NGC 4725	SABab	1206	0.675	0.802	<i>R</i>	
1941A	III	NGC 4559	SABcd	816	0.208	0.131	<i>R</i>	
1941C	II	NGC 4136	SABc	609	0.880	0.882	<i>R</i>	
1954A	Ib	NGC 4214	IABm	291	0.968	0.992	<i>R</i>	
1954C	II	NGC 5879	SABc	772	0.615	0.511	<i>R</i>	
1961I	II	NGC 4303	SABbc	1566	0.697	0.877	<i>R</i>	
1961V	'impostor*'	NGC 1058	SAC	518	0.968	0.931	<i>R</i>	Goodrich et al. (1989)
1962L	Ic	NGC 1035	SAC	1208	0.754	0.518	<i>r'</i>	
1964A	II	NGC 3631	SAC	1156	0.915	0.992	<i>R</i>	
1964F	II	NGC 4303	SABbc	1566	0.189	0.106	<i>R</i>	
1964H	II	NGC 7292	IBm	986	0.551	0.719	<i>R</i>	
1965H	IIP	NGC 4666	SABc	1529	0.324	0.198	<i>r'</i>	
1965L	IIP	NGC 3631	SAC	1156	0.622	0.658	<i>R</i>	
1965N	IIP	NGC 3074	SABc	5144	0.110	0.059	<i>R</i>	
1966B	III	NGC 4688	SBcd	986	0.571	0.454	<i>r'</i>	
1966J	Ib	NGC 3198	SBC	663	0.898	0.936	<i>R</i>	
1967H	II*	NGC 4254	SAC	2407	0.664	0.648	<i>R</i>	van Dyk (1992)
1968V	II	NGC 2276	SABc	2410	0.699	0.790	<i>R</i>	
1969B	IIP	NGC 3556	SBcd	699	0.197	0.494	<i>R</i>	
1969L	IIP	NGC 1058	SAC	518	1.000	1.000	<i>R</i>	
1971K	IIP	NGC 3811	SBcd	3105	0.809	0.900	<i>R</i>	
1971S	IIP	NGC 493	SABcd	2338	0.605	0.570	<i>R</i>	
1972Q	IIP	NGC 4254	SAC	2407	0.811	0.791	<i>R</i>	
1972R	Ib	NGC 2841	SAB	638	0.855	0.904	<i>R</i>	
1973R	IIP	NGC 3627	SABb	727	0.471	0.566	<i>R</i>	
1975T	IIP	NGC 3756	SABbc	1318	0.846	0.856	<i>R</i>	
1982F	IIP	NGC 4490	SBd	565	0.277	0.202	<i>R</i>	
1983I	Ic	NGC 4051	SABbc	700	0.498	0.473	<i>R</i>	
1984E	III	NGC 3169	SAA	1238	0.684	0.731	<i>R</i>	
1985F	Ib*	NGC 4618	SBm	544	0.121	0.087	<i>r'</i>	Gaskell et al. (1986)
1985G	IIP	NGC 4451	Sbc	864	0.138	0.212	<i>R</i>	
1985L	III	NGC 5033	SAC	875	0.585	0.571	<i>R</i>	
1986I	IIP	NGC 4254	SAC	2407	0.334	0.318	<i>R</i>	
1987F	IIn	NGC 4615	Scd	4716	0.489	0.333	<i>R</i>	
1987K	IIB	NGC 4651	SAC	805	0.409	0.303	<i>R</i>	
1987M	Ic	NGC 2715	SABc	1339	0.129	0.044	<i>R</i>	
1988L	Ib	NGC 5480	SAC	1856	0.230	0.369	<i>r'</i>	
1989C	IIP	UGC 5249	SBd	1874	0.017	0.058	<i>r'</i>	
1990E	IIP	NGC 1035	SAC	1241	0.272	0.363	<i>r'</i>	
1990H	IIP*	NGC 3294	SAC	1586	0.156	0.125	<i>R</i>	Filippenko (1993)
1990U	Ic	NGC 7479	SBC	2381	0.603	0.488	<i>R</i>	
1991A	Ic	IC 2973	SBd	3210	0.742	0.588	<i>R</i>	
1991G	IIP	NGC 4088	SABbc	757	0.466	0.453	<i>R</i>	
1991N	Ic	NGC 3310	SABbc	993	0.268	0.277	<i>R</i>	
1992C	II	NGC 3367	SBC	3040	0.689	0.687	<i>R</i>	
1993G	III*	NGC 3690	Double	3121	0.464	0.744	<i>R</i>	Tsvetkov (1994)
1993X	II	NGC 2276	SABc	2410	0.899	0.619	<i>R</i>	
1994I	Ic	NGC 5194	SABc	463		0.122	<i>R</i>	
1994Y	IIn	NGC 5371	SABbc	2558	0.355	0.212	<i>R</i>	
1994ak	IIn	NGC 2782	SABa	2543	0.725	0.977	<i>r'</i>	
1995F	Ic	NGC 2726	SABc	2410	0.037	0.050	<i>R</i>	
1995N	IIn	MCG -02-38-17	IBm	1856	0.612	0.822	<i>r'</i>	
1995V	II	NGC 1087	SABc	1517	0.368	0.497	<i>R</i>	
1995ag	II	UGC 11861	SABdm	1481	0.343	0.170	<i>R</i>	
1996ae	IIn	NGC 5775	Sb	1681	0.757	0.671	<i>R</i>	
1996ak	II	NGC 5021	SBb	8487	0.619	0.659	<i>R</i>	
1996aq	Ic	NGC 5584	SABcd	1638	0.178	0.086	<i>r'</i>	
1996bu	IIn	NGC 3631	SAC	1156	0.923	0.993	<i>R</i>	
1996cc	II	NGC 5673	SBC	2082	0.924	0.934	<i>R</i>	
1997X	Ic	NGC 4691	SB0/a	1110	0.171	0.472	<i>R</i>	
1997bs	'impostor*'	NGC 3627	SABb	727	0.362	0.348	<i>R</i>	van Dyk et al. (2000)

Table A1. Data for all SNe and host galaxies

SN	SN type	Host galaxy	Galaxy type	V_r (kms $^{-1}$)	Fr_R	$Fr_{H\alpha}$	Reference
1997db	II	UGC 11861	SABdm	1481	0.633	0.396	<i>R</i>
1997dn	II	NGC 3451	Sd	1334	0.872	0.946	<i>R</i>
1997dq	Ic*	NGC 3810	SAc	993	0.774	0.734	<i>R</i> Mazzali et al. (2004)
1997eg	IIIn	NGC 5012	SABc	2619	0.503	0.449	<i>R</i>
1997ei	Ic	NGC 3963	SABbc	3188	0.197	0.053	<i>R</i>
1998C	II	UGC 3825	SABbc	8281	0.544	0.377	<i>R</i>
1998T	Ib	NGC 3690	Double	3121	0.056	0.056	<i>R</i>
1998Y	II	NGC 2415	Im	3784	0.612	0.720	<i>R</i>
1999D	II	NGC 3690	Double	3121	0.560	0.849	<i>R</i>
1999br	IIP*	NGC 4900	SBC	960	0.786	0.932	<i>R</i> Hamuy (2003)
1999bu	Ic	NGC 3786	SABa	2678	0.180	0.522	<i>R</i>
1999bw	'impostor*'	NGC 3198	SBC	663	0.745	0.755	<i>R</i> van Dyk et al. (2005)
1999dn	Ib	NGC 3451	Sd	2798	0.872	0.946	<i>R</i>
1999ec	Ib	NGC 2207	SABbc	2741		0.521	<i>R</i>
1999el	IIIn	NGC 6951	SABbc	1424	0.320	0.259	<i>R</i>
1999em	IIP	NGC 1637	SABc	717	0.276	0.268	<i>r'</i>
1999gb	IIIn	NGC 2532	SABc	5260	0.485	0.443	<i>R</i>
1999gi	IIP	NGC 3184	SABcd	592	0.276	0.112	<i>R</i>
1999gn	IIP*	NGC 4303	SABbc	1566	0.418	0.429	<i>R</i> Pastorello et al. (2004)
2000C	Ic	NGC 2415	Im	3784	0.706	0.820	<i>R</i>
2000cr	Ic	NGC 5395	SAb	3491	0.538	0.549	<i>R</i>
2000db	II	NGC 3949	SABc	800	0.364	0.253	<i>R</i>
2000de	Ib	NGC 4384	Sa	2513	0.087	0.140	<i>R</i>
2000ew	Ic	NGC 3810	SAc	993	0.261	0.147	<i>R</i>
2001B	Ib	IC 391	SAc	1556	0.062	0.060	<i>R</i>
2001M	Ic	NGC 3240	SABb	3550	0.323	0.251	<i>R</i>
2001X	IIP	NGC 5921	SBbc	1480	0.579	0.369	<i>R</i>
2001aa	II	UGC 10888	SBb	6149	0.830	0.796	<i>R</i>
2001ac	'impostor*'	NGC 3504	SABab	1534	0.826	0.992	<i>R</i> Matheson & Calkins (2001)
2001ai	Ic	NGC 5278	SAb	7541	0.323	0.256	<i>R</i>
2001co	Ib/c	NGC 5559	SBb	5166	0.618	0.497	<i>R</i>
2001ef	Ic	IC 381	SABbc	2476	0.082	0.052	<i>R</i>
2001ej	Ib	UGC 3829	Sb	4031	0.152	0.391	<i>R</i>
2001fv	IIP*	NGC 3512	SABc	1376	0.669	0.689	<i>R</i> Matheson et al. (2001)
2001gd	IIB	NGC 5033	SAc	875	0.692	0.675	<i>R</i>
2001is	Ib	NGC 1961	SABc	3934		0.749	<i>R</i>
2002A	IIIn	UGC 3804	Scd	2887	0.419	0.253	<i>R</i>
2002bu	IIIn	NGC 4242	SABdm	506	0.896	0.930	<i>R</i>
2002ce	II	NGC 2604	SBcd	2078	0.381	0.560	<i>R</i>
2002cg	Ic	UGC 10415	SABb	9574	0.151	0.092	<i>R</i>
2002cp	Ib/c	NGC 3074	SABc	5144	0.936	0.961	<i>R</i>
2002cw	Ib	NGC 6700	SBC	4588		0.642	<i>R</i>
2002dw	II	UGC 11376	Sbc	6528	0.431	0.644	<i>R</i>
2002ed	IIP	NGC 5468	SABcd	2842	0.811	0.791	<i>R</i>
2002ei	IIP	MCG -01-09-24	Sab	2319	0.195	0.195	<i>r'</i>
2002gd	II	NGC 7537	SABc	2674	0.759	0.685	<i>R</i>
2002hn	Ic	NGC 2532	SABc	48	0.023	0.011	<i>R</i>
2002ho	Ic	NGC 4210	SBb	2732	0.146	0.051	<i>R</i>
2002ji	Ib/c	NGC 3655	SAc	1473	0.709	0.957	<i>R</i>
2002jz	Ic	UGC 2984	SBdm	1543	0.091	0.099	<i>R</i>
2003H	Ib	NGC 2207	SABbc	2741		0.259	<i>R</i>
2003T	II	UGC 4864	SAab	8368	0.682	0.643	<i>R</i>
2003Z	IIP*	NGC 2742	SAc	1289	0.675	0.736	<i>R</i> Pastorello et al. (2004)
2003ab	II	UGC 4930	Scd	8750	0.559	0.454	<i>R</i>
2003ao	IIP	NGC 2993	Sa	2430	0.456	0.784	<i>r'</i>
2003at	II	MCG +11-20-33	Sbc	7195	0.732	0.871	<i>R</i>
2003bp	Ib	NGC 2596	Sb	5938	0.486	0.362	<i>R</i>
2003db	II	MCG +05-23-21	Sc	8113	0.603	0.603	<i>R</i>
2003ed	IIB	NGC 5303	Pec	1419	0.369	0.298	<i>r'</i>
2003ef	II*	NGC 4708	SAab	4166	0.335	0.352	<i>R</i> Ganeshalingam et al. (2003)
2003el	Ic	NGC 5000	SBbc	5608	0.482	0.476	<i>R</i>
2003hp	Ic	UGC 10942	SBbc	6378	0.660	0.742	<i>R</i>
2003hr	II	NGC 2551	SA0/a	2344	0.914	1.000	<i>R</i>
2003ie	II	NGC 4051	SABbc	700	0.838	0.885	<i>R</i>

Table A1. Data for all SNe and host galaxies

SN	SN type	Host galaxy	Galaxy type	V_r (kms $^{-1}$)	Fr_R	$Fr_{H\alpha}$	Reference
2003ig	Ic	UGC 2971	Sbc	5881	0.176	0.108	<i>R</i>
2004A	IIP*	NGC 6207	SAc	852	0.729	0.660	<i>R</i>
2004C	Ic	NGC 3683	SBc	1716	0.532	0.545	<i>R</i>
2004D	II	UGC 6916	SBbc	6182	0.457	0.336	<i>R</i>
2004G	II	NGC 5668	SAd	1582	0.657	0.595	<i>R</i>
2004T	II	UGC 6038	Sb	6446	0.507	0.260	<i>R</i>
2004Z	II	MCG +10-19-85	SB0/a	6933	0.548	0.333	<i>R</i>
2004ak	II	UGC 4436	Sbc	1124	0.887	0.882	<i>R</i>
2004ao	Ib	UGC 10862	SBc	1691		0.215	<i>R</i>
2004au	II	MCG +04-42-2	Sb	7800	0.330	0.446	<i>R</i>
2004bi	Iib	UGC 5894	Sab	6537	0.875	0.846	<i>R</i>
2004bm	Ic	NGC 3437	SABc	1283	0.073	0.076	<i>R</i>
2004bn	II	NGC 3441	Sbc	6554	0.509	0.491	<i>R</i>
2004bs	Ib	NGC 3323	SBc	5164	0.191	0.119	<i>R</i>
2004dk	Ib	NGC 6118	SAd	1573	0.673	0.626	<i>R</i>
2004dg	IIP*	NGC 5806	SABb	1359	0.484	0.378	<i>R</i>
2004eb	II	NGC 6387	Pec	8499	0.413	0.540	<i>R</i>
2004ed	II	NGC 6786	SBc	7500	0.550	0.624	<i>R</i>
2004ep	II	IC 2152	SABab	1875	0.461	0.560	<i>r'</i>
2004es	II	UGC 3825	SABbc	8281	0.974	0.904	<i>r'</i>
2004ez	IIP	NGC 3430	SABc	1586	0.788	0.833	<i>r'</i>
2004gj	Iib	IC 701	SBdm	6142	0.674	0.652	<i>R</i>
2004gq	Ib	NGC 1832	SBbc	1939	0.672	0.328	<i>r'</i>
2004gr	II*	NGC 3678	Sbc	7210	0.553	0.570	<i>R</i>
2004gt	Ib/c	NGC 4038	SBm	1642	0.834	0.991	<i>r'</i>
2005D	Iib*	UGC 3856	Scd	8505	0.999	0.981	<i>R</i>
2005K	II	NGC 2923	S0/a	6538	0.743	0.784	<i>R</i>
2005O	Ib	NGC 3340	SBbc	5558	0.322	0.305	<i>R</i>
2005V	Ib/c	NGC 2146	SBab	893	0.033	0.091	<i>R</i>
2005ad	IIP	NGC 941	Sc	1608	0.831	0.864	<i>R</i>
2005az	Ic*	NGC 4961	SBcd	2535	0.426		<i>r'</i>
2005ci	II	NGC 5682	SBb	2273	0.204	0.191	<i>r'</i>
2005cs	IIP	NGC 5194	SABc	463		0.222	<i>R</i>
2005dl	II	NGC 2276	SBc	2410	0.247	0.099	<i>R</i>
2005dp	II	NGC 5630	Sdm	2655	0.534	0.590	<i>r'</i>
2005ip	II	NGC 2906	Scd	2140	0.399	0.528	<i>r'</i>
2005kk	II	NGC 3323	SBc	5164	0.766	0.875	<i>r'</i>
2005kl	Ic	NGC 4369	SAA	1045	0.271	0.540	<i>r'</i>
2005lr	Ic	ESO 492-G2	Sb	2590		0.005	<i>r'</i>
2006T	Iib	NGC 3054	SABbc	2426	0.302		<i>r'</i>
2006am	IIn	NGC 5630	Sdm	2655	0.604	0.617	<i>r'</i>
2006gi	Ib	NGC 3147	SABc	2820	0.984	0.991	<i>r'</i>
2006jc	Ib/c	UGC 4904	SB	1670	0.332	0.525	<i>r'</i>
2006ov	IIP	NGC 4303	SABbc	1566	0.418	0.429	<i>R</i>
2007C	Ib	NGC 4981	SABbc	1680	0.320	0.236	<i>R</i>
2007am	II	NGC 3367	SBc	3040	0.302	0.314	<i>r'</i>
2007fp	II	NGC 3340	SBbc	5558	0.170	0.125	<i>r'</i>
2008ax	Iib	NGC 4490	SBd	565	0.328	0.284	<i>R</i>

Table A1. Data for all SNe and host galaxies used in the analysis presented in this paper. In the first two columns the SN names and types are given. In columns 3, 4 and 5 the host galaxy names, morphological types and recession velocities are listed. Next the Fr_R and $Fr_{H\alpha}$ values derived for each SN from the above analysis are presented, and in column 8 the filter used for the observations is listed (*R*-band Johnson/Bessell or *r'*-band Sloan). In the final column a reference is given for those SNe type classifications where classification was changed from that given in the Asiago catalogue and these are also marked with an asterisk